Heterobimetallic Edge-Sharing Bioctahedral Complexes. Synthesis, Characterization, and Singlet-Triplet Separations As Determined by Phosphorus-31 Nuclear Magnetic Resonance

F. A. Cotton,* Judith L. Eglin,† Chris A. James,‡ and Rudy L. Luck§

Department of Chemistry and Laboratory for Molecular Structure and Bonding, Texas A&M University, College Station, Texas 77843

Received May 6, 1992

The heterobimetallic edge-sharing bioctahedral complexes $MoWCl_6(dppe)_2$ (**1**), $MoWCl_6(\mu\text{-dppm})_2$ (**2**), and $MoWCl_6(\mu\text{-dmpm})_2$ (**3**) are formed as the oxidative addition products of the reaction between the corresponding quadruply bonded complex and $PhICl_2$ or CH_2Cl_2. These complexes are the first examples of heteronuclear edge-sharing bioctahedral complexes of the form $MM'Cl_4(\mu\text{-Cl})_2(L\text{-}L)_2$, where L-L are bidentate phosphines. Complex **2** cocrystallizes with small amounts of $Mo_2Cl_6(\mu\text{-dppm})_2$ forming a solid solution. The apparent Mo–W distance is 2.7320 (6) Å for $MoWCl_6(\mu\text{-dppm})_2$. Complexes **1** and **3** are free from detected contamination by their dimolybdenum analogs, and the Mo–W distances are 2.7123 (9) Å for $MoWCl_6(dppe)_2$ and 2.682 (1) Å for $MoWCl_6(\mu\text{-dmpm})_2$. In addition to the structural data for these complexes, each has been fully characterized using $^{31}P\{^1H\}$ and ^1H NMR spectroscopy. Variable-temperature $^{31}P\{^1H\}$ NMR spectroscopic studies were utilized to characterize the magnetic properties of **1–3** as well as the respective homonuclear complexes. Statistical analysis of the temperature dependence of the chemical shift allows the calculation of the singlet–triplet gap ($2J$), the hyperfine coupling constant (A), and the diamagnetic shift (δ_{dia}). The crystal structures of **1–3** are fully described. Crystallographic data for these compounds are as follows: (**1**) $P2_1/n$ with a = 12.785 (3) Å, b = 12.286 (3) Å, c = 17.774 (2) Å, β = 108.598 (1)°, V = 2653 (2) Å^3, and Z = 2; (**2**) $C2/c$ with a = 23.030 (3) Å, b = 10.904 (2) Å, c = 23.2221 (3) Å, β = 124.147 (8)°, V = 4826 (1) Å^3, and Z = 4; (**3**) $P2_1/c$ with a = 7.0178 (9) Å, b = 15.526 (2) Å, c = 10.993 (2) Å, β = 94.346 (6)°, V = 1187.9 (9) Å^3, and Z = 2.

Introduction

Edge-sharing bioctahedral (ESBO) complexes constitute an important class of compounds containing multiple metal–metal bonds.[1] To the best of our knowledge, there are no known examples of heterobimetallic ESBO complexes other than those reported here.

In the past several years we have reported a variety of dimolybdenum(III) and ditungsten(III) complexes with bridging halide or thiolate ligands. The two general preparative methods for these complexes involve the oxidative addition of X_2 to quadruply bonded dinuclear complexes or the assembly of two mononuclear M(III) species to form the dinuclear complex. Obviously, only the former of these method can produce heteronuclear ESBO complexes in sufficient purity for further study. However, both these strategies have been utilized extensively in the Mo_2 and W_2 systems to produce a variety of ESBO complexes.

Despite their simplicity, the complexes are intriguing because the factors that influence the M–M bonding in these molecules are not well understood. In the simplest approximation, the metal–metal bonding in these molecules may be viewed as the overlap between metal d orbitals. One would then anticipate a set of two-centered molecular orbitals with the following energy level ordering:

$$\sigma \ll \pi < \delta < \delta^* < \pi^* \ll \sigma^*$$

A theoretical treatment of this structural type by Shaik and Hoffmann in 1980 found that an energy reversal occurs for the δ and δ^* orbitals due to mixing of the δ orbital with p orbitals on the bridging chlorine atoms. There is no similar combination of the proper symmetry to interact with the δ^* orbital, giving rise to the new energy level ordering of $\sigma \ll \pi < \delta^* < \delta < \pi^* \ll \sigma^*$ for the orbitals involved in metal–metal bonding.[2]

However, subsequent variable-temperature magnetic susceptibility measurements performed on μ-thiolate and μ-halide complexes indicated that the energies of the δ and δ^* orbitals are separated by only a few hundred to a few thousand wavenumbers. Therefore, the energy level ordering for ESBO complexes may best be regarded as $\sigma \ll \pi < \delta^* \approx \delta < \pi^* \ll \sigma^*$, resulting in a net double bond.[3]

Despite the structural and magnetic data which have been accumulated for this type of complex, the $^{31}P\{^1H\}$ NMR and ^1H NMR spectra have been reported for only one ESBO complex, $W_2Cl_6(\mu\text{-dppm})_2$.[4] The $^{31}P\{^1H\}$ NMR resonance of the phosphorus atoms of the dppm ligand, bis(diphenylphosphino)methane, was shifted to high fields, an indication of the presence of a low-lying paramagnetic excited state. In an effort to characterize complexes **1–3** more fully, we investigated the influence of the low-lying paramagnetic state on the $^{31}P\{^1H\}$ NMR chemical shifts of these complexes and their homonuclear analogs. As a result of the temperature dependence of the $^{31}P\{^1H\}$ NMR chemical shifts, we were able to evaluate the magnitude of the singlet–triplet gap of the heteronuclear complexes and revaluate the gaps for the homonuclear analogs.

Experimental Section

General Procedures. All manipulations were carried out under an atmosphere of argon unless otherwise specified. Standard Schlenk and vacuum line techniques were used. Commercial grade solvents, except alcohols and dichloro- or dibromomethane, were dried over and freshly distilled from potassium/sodium benzophenone ketyl prior to use. Alcohols and dichloro- or dibromomethane were dried over magnesium turnings and phosphorus pentoxide, respectively, and freshly dis-

† Currently at Mississippi State University, Mississippi State, MS 39762.
‡ Currently at Los Alamos National Laboratory, INC-14 MS345, Los Alamos, NM 87545.
§ Currently at The American University, Washington, D.C. 20016.

(1) Cotton, F. A. *Polyhedron* **1987**, *6*, 667.
(2) Fisel, C. R.; Hoffmann, R.; Shaik, S.; Summerville, R. H. *J. Am. Chem. Soc.* **1980**, *102*, 4555.
(3) Cotton, F. A.; Diebold, M. P.; O'Connor, C. J.; Powell, G. L. *J. Am. Chem. Soc.* **1985**, *107*, 7438.
(4) Fanwick, P. E.; Harwood, W. S.; Walton, R. A. *Inorg. Chem.* **1987**, *26*, 242.

0020-1669/92/1331-5308$03.00/0

Table I. Spectroscopic Data for Complexes 1–3

complex	$^{31}P\{^1H\}$ NMR resonances δ	^1H NMR resonances, δ	UV–vis abs, nm
$MoWCl_6(dppe)_2$ (1)	−145.3 (m, 2P, P–Mo), 174.9 (m, 2P, P–W) (J_{P-P} = 186 Hz)	8.06–7.86 (m, 40H, *Ph*P–M, M = Mo, W), 2.40 (m, 4H, CH_2P–Mo), 2.96 (m, 4H, CH_2P–W)	480
$MoWCl_6(\mu\text{-dppm})_2$ (2)	−110.6 (m, 2P, P–Mo), 105.1 (m, 2P, P–W) (J_{P-P} = 301 Hz)	7.81–6.91 (m, 40H, *Ph*P–M, M = Mo, W), 3.41 (m, 4H, CH_2P–M, M = Mo, W)	495
$MoWCl_6(\mu\text{-dmpm})_2$ (3)	−123.3 (m, 2P, P–Mo), 96.1 (m, 2P, P–W) (J_{P-P} = 309 Hz)	2.1 (m, 4H, CH_2P–M, M = Mo, W), 1.30 (m, 6H, CH_3P–Mo), 1.50 (m, 6H, CH_3P–W)	505

tilled prior to use. Phosphines were purchased from Strem Chemicals and the solids dried in vacuo prior to use. β-Mo≡$WCl_4(\mu\text{-dppe})_2$,[5] α-Mo≡$WCl_4(dppe)_2$,[5] Mo≡$WCl_4(\mu\text{-dppm})_2$,[5] $Mo_2Cl_6(dppe)_2$,[6] $W_2Cl_6(dppe)_2$,[6] $Mo_2Cl_6(\mu\text{-dppm})_2$,[7] $W_2Cl_6(\mu\text{-dppm})_2$,[8] $Mo_2Cl_6(\mu\text{-dmpm})_2$,[8] and $W_2Cl_6(\mu\text{-dmpm})_2$[8] were prepared by literature methods. Mo≡$WCl_4(PMePh_2)_4$ was prepared and purified by the literature method involving the reaction of $Mo(\eta^6\text{-}C_6H_5PMePh)(PMePh_2)_3$ with $WCl_4(PPh_3)_2$ in benzene.[9] $PhICl_2$ was prepared by combining iodobenzene and Cl_2 in chloroform.[10]

The $^{31}P\{^1H\}$ NMR (81 MHz) and ^1H NMR (200 MHz) spectra were recorded on a Varian XL-200 spectrometer. The $^{31}P\{^1H\}$ NMR chemical shift values were referenced externally and are reported relative to 85% H_3PO_4. The IR and UV–visible spectra were recorded on Perkin-Elmer 783 and Cary 17D spectrophotometers, respectively. Mass spectra were obtained from the Mass Spectrometry Applications Laboratory sponsored by the Department of Chemistry at Texas A&M University. Samples were run on a Vestec VG Analytical 70S high-resolution double-focusing magnetic sector mass spectrometer in NBA/CH_2Cl_2 matrices. The spectroscopic data for complexes 1–3 are summarized in Table I.

Preparation of $MoWCl_6(dppe)_2$ (1). Method 1. Mo≡$WCl_4(PMePh_2)_4$ (0.050 g, 0.041 mmol) and dppe (0.063 g, 0.164 mmol) were dissolved in 20 mL of THF. The reaction mixture was stirred and heated at reflux temperature for 2 h. The initial green color first turned to yellow-brown, and finally after 2 h the solution was red-brown in color. This solution was layered with hexanes and allowed to stand for several days. The resulting crystalline product (0.029 g, 58%) was found to be $MoWCl_6(dppe)_2$. The molecular ion peak in the FABMS spectrum at m/e 1290 corresponds to the $MoWCl_6(dppe)_2^+$ ion.

Method 2. A sample of α-Mo≡$WCl_4(dppe)_2$ or β-Mo≡$WCl_4(\mu\text{-dppe})_2$ (0.050 g, 0.042 mmol) was dissolved in 15 mL of THF, and $PhICl_2$ (0.020 g, 0.084 mmol) was added as the chlorinating agent. The solution immediately turned red, and a small amount of red precipitate was produced. The solvent volume was then reduced and 20 mL of hexanes added to cause complete precipitation. The red colored product was then filtered out, washed with benzene, and dried in vacuo (0.048 g, 90%).

Method 3. A sample of α-Mo≡$WCl_4(dppe)_2$ or β-Mo≡$WCl_4(\mu\text{-dppe})_2$ (0.050 g, 0.042 mmol) was dissolved in 20 mL of CH_2Cl_2 and stirred for 24 h. The initial green-brown color of the solution slowly faded and began to turn red after 2 h. The reaction mixture was stirred for an additional 22 h to ensure completion of the reaction, resulting in a red brown solution. The solvent volume was reduced in vacuo and 20 mL of hexanes added to cause precipitation of $MoWCl_6(dppe)_2$ as identified by its visible spectrum. The brown precipitate was then filtered out, washed with benzene, and dried in vacuo (0.046 g, 87%).

Table II. Crystallographic Data and Data Collection Parameters for $MoWCl_6(dppe)_2$ (1), $MoWCl_6(\mu\text{-dppm})_2$ (2), and $MoWCl_6(\mu\text{-dmpm})_2$ (3)

	1	2	3
chem formula	$WMoCl_6P_4C_{52}H_{48}$	$WMoCl_6P_4C_{50}H_{44}$	$WMoCl_6P_4C_{10}H_{28}$
fw	1289.4	1190.4	764.7
space group (no.)	$P2_1/n$ (14)	$C2/c$ (15)	$P2_1/c$ (14)
a, Å	12.785 (3)	23.030 (3)	7.0178 (9)
b, Å	12.286 (3)	10.904 (2)	15.526 (2)
c, Å	17.774 (2)	23.221 (3)	10.993 (2)
α, deg	90	90	90
β, deg	108.59 (1)	124.147 (8)	94.346 (6)
γ, deg	90	90	90
V, Å^3	2653 (2)	4826 (1)	1187.9 (9)
Z	2	4	2
T, °C	23 ± 2	23 ± 2	23 ± 2
λ, Å	0.710 73	1.541 84	1.541 84
ρ_{calcd}, g cm^{-3}	1.618	1.774	2.138
μ, cm^{-1} (Mo Kα or Cu Kα)	29.092	112.884	223.276
transm coeff	1.000–0.713 00	1.000–0.717 54	1.000–0.5726
$R(F_o)$,[a] $R_w(F_o)$[b]	0.0524, 0.0674	0.0375, 0.0410	0.033, 0.055

[a] $R = \sum||F_o| - |F_c||/\sum|F_o|$. [b] $R_w = [\sum w(|F_o| - |F_c|)^2/\sum w|F_o|^2]^{1/2}$; $w = 1/\sigma^2(|F_o|)$.

Preparation of $MoWCl_6(\mu\text{-dppm})_2$ (2). Method 1. A 0.050-g sample of Mo≡$WCl_4(\mu\text{-dppm})_2$ was dissolved in 15 mL of THF, and $PhICl_2$ (0.020 g, 0.084 mmol) was added as the chlorinating agent. The solution immediately turned red, and a small amount of red precipitate was produced. The solvent volume was then reduced and 20 mL of hexanes added to afford complete precipitation. The red product was then filtered out, washed with benzene, and dried in vacuo (0.050 g, 94%).

Method 2. A 0.050-g sample of Mo≡$WCl_4(\mu\text{-dppm})_2$ was dissolved in 20 mL of CH_2Cl_2 and stirred for 24 h. The initial green color of the solution slowly faded and began to turn red after 4 h. The reaction mixture was stirred for an additional 22 h to ensure completion of the reaction, resulting in a red solution and a small amount of red precipitate. The solution was then filtered into a Schlenk tube and layered with methanol to produce 0.040 g (75%) of microcrystalline $MoWCl_6(\mu\text{-dppm})_2$ as identified by its visible spectrum and mass spectral analysis. The molecular ion peak in the FABMS spectrum at m/e 1260 corresponds to the $MoWCl_6(\mu\text{-dppm})_2^+$ ion.

Preparation of $MoWCl_6(\mu\text{-dmpm})_2$ (3). Mo≡$WCl_4(PMePh_2)_4$ (0.050 g, 0.041 mmol) and dmpm (0.014 g, 0.1025 mmol) were suspended in a mixture of 10 mL of n-hexane and 5 mL of benzene. This suspension was stirred at ambient temperature for 1 h, and the solvents were removed in vacuo leaving an oily red-green residue. This residue was then extracted with 3 × 5 mL portions of toluene, filtered to remove any traces of the insoluble red material, and immediately cooled to −78 °C. The toluene was then removed in vacuo, and the subsequent green oily material was dissolved in CH_2Cl_2. This solution was then allowed to warm to room temperature over several hours. After the solution had reached ambient temperature it was filtered, placed in long glass tubes, and layered with a mixture of benzene and methanol (1:2). Over a period of several weeks yellow-brown crystals formed. No effort was made to optimize the yield of this reaction.

X-ray Crystallography

Single-crystal diffraction experiments were conducted using a Rigaku AFC5 automated diffractometer with Mo Kα radiation for 1 and Cu Kα radiation for 2 and 3. Routine unit cell identification and intensity data collection procedures were followed utilizing the options specified in Table II and the general procedures previously described.[11] Lattice dimensions and Laue symmetry were verified using axial photographs. Three standard reflections were measured every 1 h during data collections to monitor any gain or loss in intensity and a correction applied when ΔI was greater than 5%. Corrections for Lorentz, polarization, and absorption effects

(5) Cotton, F. A.; James, C. A. *Inorg. Chem.*, preceding paper in this issue.
(6) Agaskar, P. A.; Cotton, F. A.; Dunbar, K. R.; Falvello, L. R.; O'Connor, C. J. *Inorg. Chem.* **1987**, *26*, 4051.
(7) Chakravarty, A. R.; Cotton, F. A.; Diebold, M. P.; Lewis, D. B.; Roth, W. J. *J. Am. Chem. Soc.* **1986**, *108*, 971.
(8) Canich, J. M.; Cotton, F. A.; Daniels, L. M.; Lewis, D. B. *Inorg. Chem.* **1987**, *26*, 4046.
(9) Luck, R. L.; Morris, R. H.; Sawyer, J. F. *Inorg. Chem.* **1987**, *26*, 2422.
(10) Kennedy, E. R.; Lucas, H. J. *Organic Syntheses*; Wiley: New York, 1955; Collect. Vol. 3, p 482.
(11) Bino, A.; Cotton, F. A.; Fanwick, P. E. *Inorg. Chem.* **1979**, *18*, 3558.

were applied to all data sets. The latter correction was based on azumuthal scans of several reflections with the diffractometer angle χ near 90°.[12]

General Solution and Refinement. The following general procedures were employed for the solution and refinement of all compounds unless otherwise noted.

The heavy-atom positions were obtained from three-dimensional Patterson functions. Hybrid atoms (MW) composed of 50% Mo and 50% W were placed at the metal atom positions in the initial stages of the refinement. The positions for the remainder of the non-hydrogen atoms were found using a series of full matrix refinements followed by difference Fourier syntheses. These positions were initially refined with isotropic thermal parameters and then with anisotropic thermal parameters to convergence. The hydrogen atoms, where included, were placed and fixed at calculated positions and their isotropic thermal parameters constrained to one variable, and the entire model refined to convergence. Final refinements employed the SHELX-76 package of programs with variations in occupancy factors used to determine the composition of the metal atom sites. Important details pertinent to individual compounds are presented in Table II and in the following paragraphs.

Compound 1. Crystals of $MoWCl_6(dppe)_2$ were obtained as described in the Experimental Section. A red-brown platelike crystal was selected and mounted on the end of a glass fiber with epoxy cement.

Systematic absences uniquely determined the space group as $P2_1/n$. The difference Fourier map showed only "ghost" peaks in close proximity to the heavy-atom positions. The residuals, at convergence with isotropic thermal parameters, were $R = 0.1193$ and $R_w = 0.1434$. Because the residuals remained high at this point in the refinement, a calculated absorption correction utilizing the DIFABS[13] program was applied to the data set. After the application of this correction, the model was allowed to refine freely first with isotropic and then finally anisotropic thermal parameters to convergence. The initial refinement of the hybrid metal atom composition, the mass spectral analysis, and the $^{31}P\{^1H\}$ NMR analysis failed to indicated the presence of $Mo_2Cl_6(dppe)_2$. Therefore, the hybrid metal atom composition was fixed at 50.0% Mo and 50.0% W in the final refinement. The final refinement factors after convergence are listed in Table II. Table III contains positional and thermal parameters for non-hydrogen atoms. Selected bond lengths and angles are listed in Table IV. An ORTEP diagram of the molecule is given in Figure 1. Tables of anisotropic thermal parameters, complete bond lengths and angles, and hydrogen atom positional parameters and a complete ORTEP diagram are available as supplementary material.

Compound 2. Crystals of $MoWCl_6(\mu\text{-dppm})_2$ were obtained by layering a dilute CH_2Cl_2 solution of this compound with a mixture of benzene and methanol (1:2) in a long glass tube sealed under an argon atmosphere. A red needle-shaped crystal was selected from the tube and mounted on the end of a glass fiber with epoxy cement.

Systematic absences narrowed the choice of space groups to $C2/c$ or Cc. The centrosymmetric space group, $C2/c$, was selected for the initial refinement, and this choice proved satifactory. The final difference Fourier showed only one peak above 1 e/Å^3. The composition of the hybrid metal atom was 59.4 (6)% Mo and 40.6 (6)% W in the final refinement and was in reasonable agreement with the $^{31}P\{^1H\}$ NMR spectrum of a solution of the crystals which indicated the presence of ca. 20% $Mo_2Cl_6(\mu\text{-dppm})_2$. The final refinement factors after convergence are listed in Table II. Table V contains positional and thermal parameters for non-hydrogen atoms. Selected bond lengths and angles are listed in Table VI, and an ORTEP diagram of the molecule is given in Figure 2. Tables of anisotropic thermal parameters, complete bond lengths and angles, and hydrogen atom positional parameters and a complete ORTEP drawing are available as supplementary material.

Compound 3. Crystals of $MoWCl_6(\mu\text{-dmpm})_2$ were obtained as described in the Experimental Section. A yellow-brown blocklike crystal was selected, coated with epoxy cement, and mounted on the end of a glass fiber. The standards monitored during data collection indicated the crystal had decayed 4.5%. The data set was subsequently corrected for the decay.

Systematic absences unambiguously identified the space group as $P2_1/c$. The final difference Fourier map contained no peaks above 1 e/Å^3, and no effort was made to include the hydrogen atoms. Because both the initial refinement of the hybrid metal atom composition and the $^{31}P\{^1H\}$ NMR spectral analysis failed to indicate the presence of $Mo_2Cl_6(\mu\text{-dmpm})_2$, the hybrid metal atom composition was fixed at 50.0% Mo and 50.0% W in the final refinement. The final refinement factors after convergence are listed in Table II. Table VII contains positional and thermal parameters for non-hydrogen atoms. Complete bond lengths and angles are listed in Table VIII. An ORTEP diagram of the molecule is given in Figure 3. Tables of anisotropic thermal parameters are available as supplementary material.

Table III. Positional and Thermal Parameters for Non-Hydrogen Atoms of $MoWCl_6(dppe)_2$ (1)

atom	x	y	z	B,[a] Å^2
MoW(1)[b]	0.44954 (4)	0.03874 (5)	0.05104 (3)	2.00 (2)
Cl(1)	0.6124 (2)	0.0828 (2)	0.1588 (2)	3.10 (7)
Cl(2)	0.5056 (2)	0.1496 (2)	−0.0412 (2)	2.79 (7)
Cl(3)	0.2617 (2)	0.0143 (3)	−0.0314 (2)	3.29 (7)
P(1)	0.3828 (2)	−0.0296 (3)	0.1629 (2)	2.61 (7)
P(2)	0.3812 (2)	0.2188 (3)	0.0883 (2)	2.61 (7)
C(11)	0.368 (1)	0.091 (1)	0.2175 (7)	3.9 (3)
C(22)	0.310 (1)	0.185 (1)	0.1614 (8)	4.3 (4)
C(121)	0.4685 (6)	−0.1190 (7)	0.2420 (4)	2.9 (3)
C(122)	0.5727 (6)	−0.1547 (7)	0.2433 (4)	4.2 (3)
C(123)	0.6334 (6)	−0.2241 (7)	0.3035 (4)	5.5 (4)
C(124)	0.5900 (6)	−0.2578 (7)	0.3624 (4)	5.5 (4)
C(125)	0.4858 (6)	−0.2221 (7)	0.3611 (4)	6.7 (5)
C(126)	0.4251 (6)	−0.1527 (7)	0.3009 (4)	5.1 (4)
C(131)	0.2494 (8)	−0.0981 (9)	0.1338 (8)	4.7 (4)
C(132)	0.1523 (8)	−0.0453 (9)	0.1326 (8)	9.8 (8)
C(133)	0.0519 (8)	−0.1008 (9)	0.1073 (8)	14 (1)
C(134)	0.0486 (8)	−0.2092 (9)	0.0832 (8)	13 (1)
C(135)	0.1457 (8)	−0.2620 (9)	0.0844 (8)	14 (1)
C(136)	0.2461 (8)	−0.2065 (9)	0.1097 (8)	8.8 (7)
C(211)	0.2777 (7)	0.2993 (6)	0.0142 (5)	3.6 (3)
C(212)	0.2546 (7)	0.2804 (6)	−0.0669 (5)	4.3 (3)
C(213)	0.1817 (7)	0.3486 (6)	−0.1220 (5)	5.1 (4)
C(214)	0.1319 (7)	0.4355 (6)	−0.0961 (5)	6.8 (5)
C(215)	0.1550 (7)	0.4543 (6)	−0.0150 (5)	9.1 (7)
C(216)	0.2279 (7)	0.3862 (6)	0.0401 (5)	5.8 (4)
C(221)	0.4834 (9)	0.3220 (8)	0.1338 (5)	3.7 (3)
C(222)	0.5190 (9)	0.3442 (8)	0.2150 (5)	7.6 (6)
C(223)	0.5971 (9)	0.4256 (8)	0.2456 (5)	8.5 (7)
C(224)	0.6395 (9)	0.4848 (8)	0.1949 (5)	9.4 (7)
C(225)	0.6039 (9)	0.4627 (8)	0.1137 (5)	8.9 (7)
C(226)	0.5259 (9)	0.3812 (8)	0.0832 (5)	6.2 (5)

[a] Anisotropically refined atoms are given in the form of the equivalent isotropic displacement parameter defined as $^1/_3[a^2a^{*2}B_{11} + b^2b^{*2}B_{22} + c^2c^{*2}B_{33} + 2ab(\cos\gamma)a^*b^*B_{12} + 2ac(\cos\beta)a^*c^*B_{13} + 2bc(\cos\alpha)b^*c^*B_{23}]$. [b] Hybrid metal atom composed of 50.0% Mo and 50.0% W.

Table IV. Selected Bond Lengths (Å) and Angles (deg) for $MoWCl_6(dppe)_2$ (1)[a]

Distances			
MW(1)[b]–MW(1)	2.7123 (9)	P(1)–C(11)	1.81 (1)
MW(1)–Cl(2)	2.399 (2)	P(1)–C(121)	1.843 (8)
MW(1)–Cl(1)	2.411 (3)	P(1)–C(131)	1.82 (1)
MW(1)–Cl(1)	2.404 (3)	P(2)–C(22)	1.86 (2)
MW(1)–Cl(3)	2.400 (2)	P(2)–C(211)	1.831 (8)
MW(1)–P(1)	2.544 (3)	P(2)–C(221)	1.82 (1)
MW(1)–P(2)	2.542 (3)	C(11)–C(22)	1.56 (2)
Angles			
MW(1)–MW(1)–Cl(2)	97.83 (8)	Cl(1)–MW(1)–P(2)	83.5 (1)
MW(1)–MW(1)–Cl(1)	55.59 (7)	Cl(1)–MW(1)–Cl(3)	92.9 (1)
MW(1)–MW(1)–Cl(1)	55.83 (8)	Cl(1)–MW(1)–P(1)	83.4 (1)
MW(1)–MW(1)–Cl(3)	98.30 (8)	Cl(1)–MW(1)–P(2)	165.1 (1)
MW(1)–MW(1)–P(1)	139.18 (8)	Cl(3)–MW(1)–P(1)	85.2 (1)
MW(1)–MW(1)–P(2)	139.09 (8)	Cl(3)–MW(1)–P(2)	84.7 (1)
Cl(2)–MW(1)–Cl(1)	92.58 (9)	P(1)–MW(1)–P(2)	81.7 (1)
Cl(2)–MW(1)–Cl(1)	96.24 (9)	MW(1)–Cl(1)–MW(1)	68.58 (8)
Cl(2)–MW(1)–Cl(3)	163.9 (1)	C(11)–P(1)–C(121)	102.4 (4)
Cl(2)–MW(1)–P(1)	82.67 (9)	C(11)–P(1)–C(131)	106.4 (6)
Cl(2)–MW(1)–P(2)	83.04 (9)	C(121)–P(1)–C(131)	102.5 (5)
Cl(1)–MW(1)–Cl(1)	111.4 (1)	C(22)–P(2)–C(211)	102.7 (5)
Cl(1)–MW(1)–Cl(3)	96.4 (1)	C(22)–P(2)–C(221)	106.6 (5)
Cl(1)–MW(1)–P(1)	164.9 (1)	C(211)–P(2)–C(221)	101.3 (4)

[a] Numbers in parentheses are estimated standard deviations in the least significant digit. [b] Hybrid metal atom composed of 50.0% Mo and 50.0% W.

(12) North, A. C. T.; Phillips, D. A.; Matthews, F. S. *Acta Crystallogr., Sect. A: Cryst. Phys., Diffr., Theor. Gen. Crystallogr.* **1968**, *24A*, 351.
(13) North, A. C. T.; Phillips, D. A.; Matthews, F. S. *Acta Crystallogr.* **1983**, *A39*, 159.

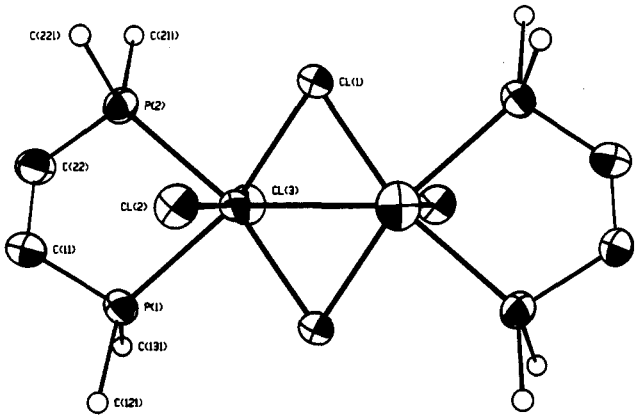

Figure 1. ORTEP drawing of $MoWCl_6(dppe)_2$ (phenyl rings of dppe omitted). Thermal ellipsoids, except phenyl carbons, are drawn at 50% probability.

Table V. Positional and Thermal Parameters for Non-Hydrogen Atoms of $MoWCl_6(\mu\text{-dppm})_2$ (**2**)

atom	x	y	z	B,[a] Å^2
MW(1)[b]	0.06424 (2)	0.05061 (5)	0.02614 (2)	2.52 (2)
Cl(1)	0.0454 (1)	−0.1466 (2)	0.0588 (1)	3.38 (7)
Cl(2)	0.1112 (1)	0.2453 (2)	0.0215 (1)	4.22 (8)
Cl(3)	0.1853 (1)	−0.0093 (2)	0.0989 (1)	4.34 (8)
P(1)	0.0734 (1)	0.1363 (2)	0.1346 (1)	3.09 (7)
P(2)	0.0695 (1)	−0.0234 (2)	−0.0764 (1)	3.22 (7)
C(1)	0.0203 (4)	0.0452 (9)	0.1548 (4)	3.5 (3)
C(111)	0.1606 (4)	0.1242 (6)	0.2138 (4)	3.9 (3)
C(112)	0.2080 (4)	0.2164 (6)	0.2253 (4)	7.8 (5)
C(113)	0.2770 (4)	0.2113 (6)	0.2835 (4)	10.8 (7)
C(114)	0.2987 (4)	0.1138 (6)	0.3302 (4)	7.6 (5)
C(115)	0.2514 (4)	0.0216 (6)	0.3187 (4)	6.1 (4)
C(116)	0.1823 (4)	0.0267 (6)	0.2605 (4)	4.8 (4)
C(121)	0.0494 (6)	0.2926 (7)	0.1375 (3)	4.4 (4)
C(122)	0.0619 (6)	0.3385 (7)	0.1995 (3)	11 (1)
C(123)	0.0442 (6)	0.4594 (7)	0.2029 (3)	14 (1)
C(124)	0.0140 (6)	0.5343 (7)	0.1442 (3)	9 (1)
C(125)	0.0015 (6)	0.4884 (7)	0.0821 (3)	6.1 (5)
C(126)	0.0193 (6)	0.3675 (7)	0.0788 (3)	4.7 (4)
C(211)	0.1071 (3)	0.0895 (8)	−0.1041 (4)	3.8 (3)
C(212)	0.1800 (3)	0.1009 (8)	−0.0633 (4)	7.6 (5)
C(213)	0.2124 (3)	0.1877 (8)	−0.0805 (4)	8.6 (7)
C(214)	0.1719 (3)	0.2630 (8)	−0.1385 (4)	7.0 (6)
C(215)	0.0990 (3)	0.2515 (8)	−0.1792 (4)	7.6 (6)
C(216)	0.0666 (3)	0.1647 (8)	−0.1620 (4)	6.2 (4)
C(221)	0.1168 (4)	−0.1612 (7)	−0.0705 (3)	4.4 (3)
C(222)	0.1306 (4)	−0.1840 (7)	−0.1209 (3)	7.2 (5)
C(223)	0.1633 (4)	−0.2930 (7)	−0.1191 (3)	9.1 (6)
C(224)	0.1822 (4)	−0.3792 (7)	−0.0670 (3)	7.0 (5)
C(225)	0.1684 (4)	−0.3564 (7)	−0.0167 (3)	5.4 (4)
C(226)	0.1357 (4)	−0.2474 (7)	−0.0184 (3)	4.6 (4)

[a] Anisotropically refined atoms are given in the form of the equivalent isotropic displacement parameter defined as $^1/_3[a^2a^{*2}B_{11} + b^2b^{*2}B_{22} + c^2c^{*2}B_{33} + 2ab(\cos\gamma)a^*b^*B_{12} + 2ac(\cos\beta)a^*c^*B_{13} + 2bc(\cos\alpha)b^*c^*B_{23}]$. [b] Hybrid metal atom composed of 59.4 (6)% Mo and 40.6 (6)% W.

Table VI. Selected Bond Lengths (Å) and Angles (deg) for $MoWCl_6(\mu\text{-dppm})_2$ (**2**)[a]

MW(1)[b]–MW(1)	2.7230 (6)	P(1)–C(1)	1.83 (1)
MW(1)–Cl(1)	2.399 (2)	P(1)–C(111)	1.814 (6)
MW(1)–Cl(1)	2.402 (2)	P(1)–C(121)	1.804 (9)
MW(1)–Cl(2)	2.412 (3)	P(2)–C(1)	1.849 (7)
MW(1)–Cl(3)	2.401 (2)	P(2)–C(211)	1.82 (1)
MW(1)–P(1)	2.581 (3)	P(2)–C(221)	1.816 (9)
MW(1)–P(2)	2.581 (3)		

Angles

MW(1)–MW(1)–Cl(1)	55.48 (5)	Cl(1)–MW(1)–P(2)	87.15 (8)
MW(1)–MW(1)–Cl(1)	55.41 (6)	Cl(2)–MW(1)–Cl(3)	84.17 (8)
MW(1)–MW(1)–Cl(2)	137.63 (5)	Cl(2)–MW(1)–P(1)	86.1 (1)
MW(1)–MW(1)–Cl(3)	138.19 (7)	Cl(2)–MW(1)–P(2)	88.8 (1)
MW(1)–MW(1)–P(1)	93.14 (6)	Cl(3)–MW(1)–P(1)	89.17 (8)
MW(1)–MW(1)–P(2)	93.66 (5)	Cl(3)–MW(1)–P(2)	85.81 (9)
Cl(1)–MW(1)–Cl(1)	110.89 (7)	P(1)–MW(1)–P(2)	173.20 (8)
Cl(1)–MW(1)–Cl(2)	165.49 (6)	MW(1)–Cl(1)–MW(1)	69.11 (5)
Cl(1)–MW(1)–Cl(3)	83.04 (8)	C(1)–P(1)–C(111)	102.7 (4)
Cl(1)–MW(1)–P(1)	86.89 (8)	C(1)–P(1)–C(121)	103.9 (5)
Cl(1)–MW(1)–P(2)	97.02 (8)	C(111)–P(1)–C(121)	102.6 (3)
Cl(1)–MW(1)–Cl(2)	82.56 (7)	C(1)–P(2)–C(211)	103.3 (4)
Cl(1)–MW(1)–Cl(3)	165.1 (1)	C(1)–P(2)–C(221)	105.1 (4)
Cl(1)–MW(1)–P(1)	96.68 (8)	C(211)–P(2)–C(221)	101.6 (4)

[a] Numbers in parentheses are estimated standard deviations in the least significant digit. [b] Hybrid metal atom composed of 59.4 (6)% Mo and 40.6 (6)% W.

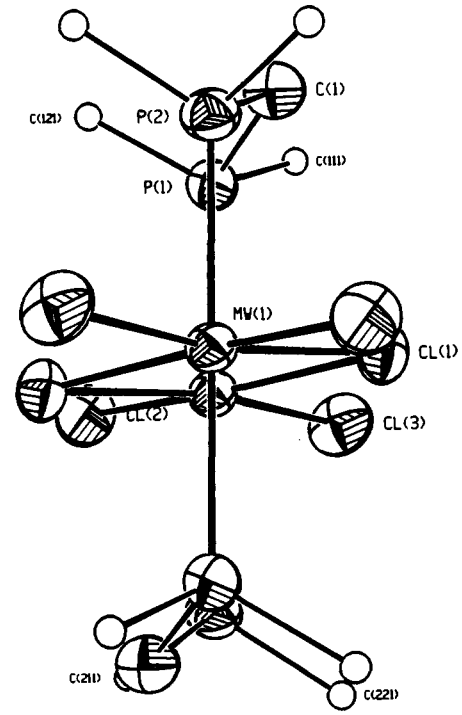

Figure 2. ORTEP drawing of $MoWCl_6(\mu\text{-dppm})_2$ (phenyl rings of dppm omitted). Thermal ellipsoids, except phenyl carbons, are drawn at 50% probability.

Results and Discussion

Synthesis. The preparation of complexes **1**–**3** proceeds straightforwardly via oxidative addition of $PhICl_2$, phenyldichloroiodine(III), to the appropriate quadruply bonded species. However, if any of the analogous dimolybdenum complexes are present, they are also oxidized, and mixtures of $MoWCl_6(L\text{-}L)_2$ and $Mo_2Cl_6(L\text{-}L)_2$ are nearly impossible to separate. A more selective oxidant for the $Mo\equiv^4W$ core is CH_2Cl_2. When solutions of $Mo\equiv^4W$ complexes in CH_2Cl_2 are stirred for several hours at room temperature, the dichloromethane oxidizes only the $Mo\equiv^4W$ complexes to $MoWCl_6$ type complexes, leaving the $Mo\equiv^4Mo$ complexes unchanged. The propensity of the W_2^{4+} core to undergo oxidative addition under acidic as well as nonacidic conditions has been established,[4,8,14,15] and the analogous ditungsten systems are also sensitive to oxidation by dichloromethane. This selectivity is presumably a result of the difference in the oxidation potentials of the Mo_2, MoW, W_2 triad.[9,16,17] This and other observations indicate that the chemistry of the mixed-metal compound is more closely related to that of the W_2 compound than to that of the Mo_2 compound.

(14) Huffman, J. C.; McLaughlin, K. W.; Sattelberger, A. P. *J. Am. Chem. Soc.* **1981**, *103*, 2280.
(15) Cotton, F. A.; Mott, G. N. *J. Am. Chem. Soc.* **1982**, *104*, 5978.
(16) Morris, R. H. *Polyhedron* **1987**, *6*, 793.
(17) Klendworth, D. D.; Nimroy, T.; Salmon, D. J.; Walton, R. A.; Zeitlow, T. C. *Inorg. Chem.* **1981**, *20*, 947.

Table VII. Positional and Thermal Parameters for Non-Hydrogen Atoms of $MoWCl_6(\mu\text{-dmpm})_2$ (3)

atom	x	y	z	B,[a] Å^2
MW(1)[b]	0.0558 (1)	0.05917 (6)	0.0846 (1)	3 (1)
Cl(1)	−0.0584 (8)	0.1229 (4)	0.2694 (6)	5 (6)
Cl(2)	0.3274 (8)	0.1547 (4)	0.1253 (5)	5 (6)
Cl(3)	0.2464 (7)	0.0107 (3)	−0.0728 (5)	4 (5)
P(1)	0.2040 (7)	−0.0496 (4)	0.2336 (5)	4 (5)
P(2)	−0.0892 (7)	0.1835 (3)	−0.0407 (5)	3 (5)
C(1)	0.581 (3)	0.015 (2)	0.673 (2)	5 (8)
C(2)	0.054 (4)	−0.086 (2)	0.352 (2)	5 (8)
C(3)	0.277 (3)	−0.149 (1)	0.158 (2)	4 (4)
C(4)	0.082 (3)	0.244 (2)	−0.122 (2)	5 (7)
C(6)	0.286 (3)	0.235 (2)	0.542 (2)	5 (7)

[a] Anisotropically refined atoms are given in the form of the equivalent isotropic displacement parameter defined as $^1/_3[a^2a^{*2}B_{11} + b^2b^{*2}B_{22} + c^2c^{*2}B_{33} + 2ab(\cos\gamma)a^*b^*B_{12} + 2ac(\cos\beta)a^*c^*B_{13} + 2bc(\cos\alpha)b^*c^*B_{23}]$. [b] Hybrid metal atom composed of 50.0% Mo and 50.0% W.

Table VIII. Complete Bond Lengths (Å) and Angles (deg) for $MoWCl_6(\mu\text{-dmpm})_2$ (3)[a]

MW(1)[b]-MW(1)	2.682 (1)	P(1)-C(1)	1.84 (2)
MW(1)-Cl(3)	2.439 (6)	P(1)-C(2)	1.82 (3)
MW(1)-Cl(2)	2.430 (6)	P(1)-C(3)	1.84 (2)
MW(1)-Cl(1)	2.380 (5)	P(2)-C(3)	1.85 (2)
MW(1)-Cl(1)	2.376 (5)	P(2)-C(4)	1.81 (3)
MW(1)-P(1)	2.516 (5)	P(2)-C(6)	1.82 (3)
MW(1)-P(2)	2.535 (5)		

Angles

MW(1)-MW(1)-Cl(3)	138.8 (1)	Cl(1)-MW(1)-P(1)	93.0 (2)
MW(1)-MW(1)-Cl(2)	136.8 (1)	Cl(1)-MW(1)-P(2)	89.9 (2)
MW(1)-MW(1)-Cl(1)	55.6 (1)	P(1)-MW(1)-P(2)	172.0 (2)
MW(1)-MW(1)-Cl(1)	55.8 (1)	MW(1)-Cl(1)-MW(1)	68.6 (1)
MW(1)-MW(1)-P(1)	94.1 (1)	MW(1)-P(1)-C(1)	116.4 (8)
MW(1)-MW(1)-P(2)	93.7 (1)	MW(1)-P(1)-C(2)	115.9 (8)
Cl(3)-MW(1)-Cl(2)	84.4 (2)	MW(1)-P(1)-C(3)	112.6 (7)
Cl(3)-MW(1)-Cl(1)	164.8 (2)	C(1)-P(1)-C(2)	101 (1)
Cl(3)-MW(1)-Cl(1)	83.2 (2)	C(1)-P(1)-C(3)	105 (1)
Cl(3)-MW(1)-P(1)	83.2 (2)	C(2)-P(1)-C(3)	105 (1)
Cl(3)-MW(1)-P(2)	89.7 (2)	MW(1)-P(2)-C(3)	112.7 (7)
Cl(2)-MW(1)-Cl(1)	81.3 (2)	MW(1)-P(2)-C(4)	114.0 (8)
Cl(2)-MW(1)-Cl(1)	166.6 (2)	MW(1)-P(2)-C(6)	116.8 (8)
Cl(2)-MW(1)-P(1)	90.6 (2)	C(3)-P(2)-C(4)	106 (1)
Cl(2)-MW(1)-P(2)	84.9 (2)	C(3)-P(2)-C(6)	102 (1)
Cl(1)-MW(1)-Cl(1)	111.4 (2)	C(4)-P(2)-C(6)	104 (1)
Cl(1)-MW(1)-P(1)	91.6 (2)	P(1)-C(3)-P(2)	111 (1)
Cl(1)-MW(1)-P(2)	94.3 (2)		

[a] Numbers in parentheses are estimated standard deviations in the least significant digit. [b] Hybrid metal atom composed of 50.0% Mo and 50.0% W.

The mechanism by which this oxidation occurs has not been established but may be one of the following processes: (1) Formation of Cl and CH_2Cl radicals followed by the reaction of the quadruply bonded complex and the Cl radical; (2) direct reaction of CH_2Cl_2 with the quadruply bonded complex and subsequent cleavage of the Cl–C bond producing CH_2Cl radicals; (3) oxidative addition of CH_2Cl_2 to the quadruple bond forming $[M_2Cl_5(L\text{-}L)_2(CH_2Cl)]$. This species might then react with another molecule of CH_2Cl_2 forming $M_2X_6(L\text{-}L)_2$ and liberating $Cl_2(CH_2)_2$.

The formation of $MoWCl_6(dppe)_2$ from $Mo\equiv WCl_4(PMePh_2)_4$ and dppe in refluxing THF leaves many questions concerning the source and nature of the oxidizing agent. There are other examples of the MoW^{4+} core being oxidized to MoW^{6+} in the absence of added oxidant.[18,19] In the current case, either chloride-containing impurities in the starting material or a disproportionation reaction are the most plausible sources for the oxidant.

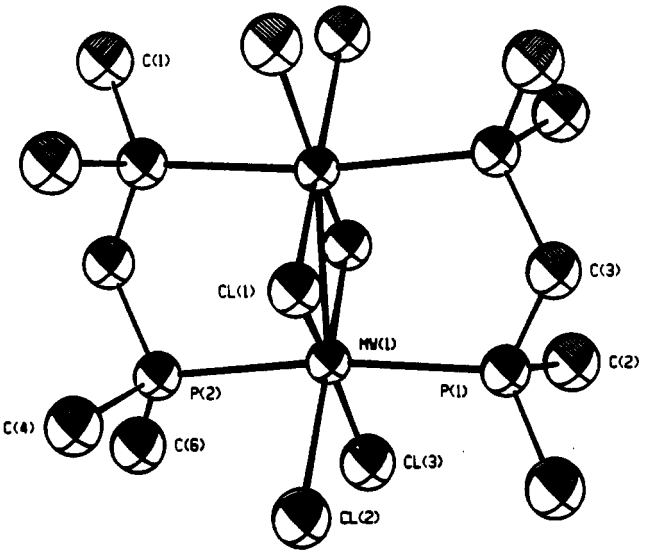

Figure 3. ORTEP drawing of $MoWCl_6(\mu\text{-dmpm})_2$ (phenyl rings of dmpm omitted). Thermal ellipsoids are drawn at 50% probability.

Structure and Bonding. The $M_2X_6(L\text{-}L)_2$ compounds reported here have been characterized by X-ray crystallography. The molecules possess geometries based on an edge-sharing bioctahedral arrangement of the core atoms. In complex **1**, the $MM'Cl_6P_4$ unit is arranged so that the equatorial plane is occupied by chelating diphosphines and bridging chloride ions and the four apical positions are filled by terminal chloride ligands. In the case of **2** and **3**, the central $MM'Cl_6P_4$ core unit has essentially the same structure but the equatorial plane is occupied by terminal and bridging chloride ligands and the four apical positions are filled by bridging diphosphines. The bond angles around the metal atoms are those of an octahedral arrangement distorted in the usual manner because of the presence of metal–metal bonding, viz., opening of the (μ-X)–M–(μ-X) angle and deviation from linearity of the angle Cl_t–M–Cl_t.[1]

The crystals structures of **1–3** show the usual type of disorder (i.e., random arrangement) generally observed in heteronuclear systems. Therefore, the metal to ligand bond distances are averages of the Mo–L and W–L (L = Cl or P) distances due to the random arrangement of the M–M′ vector.[16] Because of this averaging, only the metal–metal bond lengths and overall conformations of **1–3** may be determined precisely.[9,20–22]

The specific characteristics of each complex and the relationships between them will be explored in the following paragraphs.

Compound 1. The structural characterization of $MoWCl_6(dppe)_2$ revealed little that was unexpected. This complex is isomorphous with the dimolybdenum and ditungsten analogs with only slight variations in bond lengths and angles.[8] The metal–metal bond length of 2.7123 (9) Å and M–Cl_b–M angle of 68.58 (8)° are both indicative of some degree of metal–metal bonding. Selected bond distances and angles are listed in Table IV, and a complete ORTEP drawing is shown in Figure 1.

Compound 2. This compound is also similar to its dimolybdenum and ditungsten counterparts.[7,8] However, there is one subtle difference in the structural data. The crystal used for the X-ray diffraction experiment and the bulk product were found to contain small amounts of $Mo_2Cl_6(\mu\text{-dppm})_2$. In other words, the two compounds form a solid solution.[23] This is not surprising considering that the $Mo\equiv WCl_4(\mu\text{-dppm})_2$ used in the preparation of **2** was found to contain the same percentage of

(18) Cotton, F. A.; Luck, R. L.; James, C. A. *Inorg. Chem.* **1991**, *30*, 4370.
(19) Katovic, V.; McCarley, R. E. *Inorg. Chem.* **1978**, *17*, 1268.
(20) Cotton, F. A.; Hanson, B. E. *Inorg. Chem.* **1978**, *17*, 3237.
(21) Katovic, V.; McCarley, R. E. *J. Am. Chem. Soc.* **1978**, *100*, 5586.
(22) Garner, C. D.; Senior, R. G.; King, T. J. *J. Am. Chem. Soc.* **1976**, *98*, 3526.
(23) Cotton, F. A.; Lewis, G. E.; Murillo, C. A.; Schwotzer, W.; Valle, G. *Inorg. Chem.* **1984**, *23*, 4038.

Table IX. Comparison of Important Structural Dimensions (Å, deg) between $MM'Cl_4(\mu\text{-}Cl)_2(L\text{-}L)_2$ Complexes, Where L-L = dppm, dppe, and dmpm

	$MoWCl_6(L\text{-}L)_2$			$Mo_2Cl_6(L\text{-}L)_2$			$W_2Cl_6(L\text{-}L)_2$		
bond or angle	dppm	dppe	dmpm	dppm[7]	dppe[6]	dmpm	dppm[8]	dppe[6]	dmpm
M–M′	2.7320 (6)	2.7123 (9)	2.682 (1)	2.789 (1)	2.762 (1)	2.7394 (5)	2.691 (1)	2.682 (1)	2.6663 (4)
M–P(av)	2.581 (3)	2.543 (3)	2.526 (5)	2.586 (2)	2.556 (2)	2.552 (2)	2.564 (3)	2.530 (4)	2.534 (2)
M–Cl_b(av)	2.400 (2)	2.407 (3)	2.376 (5)	2.403 (2)	2.417 (2)	2.390 (3)	2.399 (3)	2.404 (3)	2.385 (2)
M–Cl_t(av)	2.406 (3)	2.400 (2)	2.435 (6)	2.400 (2)	2.396 (2)	2.428 (2)	2.410 (4)	2.394 (4)	2.439 (2)
Cl_t–M–Cl_t(av)	84.17 (8)	163.9 (1)	84.4 (2)	84.55 (8)	164.97 (3)	84.70 (4)	84.1 (1)	164.2 (7)	84.23 (7)
Cl_b–M–Cl_b(av)	110.89 (6)	111.4 (1)	111.89 (2)	109.08 (5)	110.32 (5)	110.05 (2)	111.77 (9)	112.1 (2)	112.03 (6)
P–M–P(av)	173.20 (8)	81.7 (1)	172.0 (2)	174.41 (7)	81.25 (6)			82.0 (1)	
M–Cl_b–M(av)	69.11 (5)	68.6 (1)	68.6 (1)	70.92 (5)	69.68 (6)	69.95 (2)	68.23 (9)	67.8 (1)	67.97 (5)

Mo–$MoCl_4(\mu\text{-dppm})_2$. Solid solutions are not uncommon and have been reported for several mononuclear[23] and quadruply bonded heteronuclear systems.[9,24] Again, the metal–metal bond length of 2.7320 (6) Å and the M–Cl_b–M angle of 69.11 (5)° are both indicative of some degree of metal–metal bonding. Selected bond distances and angles are listed in Table VI, and a complete ORTEP drawing is shown in Figure 2.

Compound 3. Again the structural characterization of $MoWCl_6(\mu\text{-dppm})_2$ produced little that is different from the analogous dimolybdenum and ditungsten complexes. Nearly all the structural parameters are an average of those for $Mo_2Cl_6(\mu\text{-dmpm})_2$ and $W_2Cl_6(\mu\text{-dmpm})_2$.[8] The metal–metal bond length of 2.682 (1) Å and the M–Cl_b–M angle of 68.6 (1)° both indicated a stronger metal–metal interaction than in complex **2**. These differences will be examined more carefully in the following paragraphs. Selected bond distances and angles are listed in Table VIII, and a complete ORTEP drawing is shown in Figure 3.

Heteronuclear vs Homonuclear. As the number of heteronuclear compounds grows, it becomes apparent that the structural characteristics of these complexes are often an average of the respective homonuclear analogs.[9,16,24] The ESBO complexes reported here are no exception. If one employs the formal shortness ratio (FSR),[25,26] which has been used for the comparison of metal–metal bond distances in quadruply bonded complexes, the metal–metal bond distances for the ESBO species may be more easily evaluated. Structural data for the Mo_2, MoW, W_2 triad of ESBO complexes are complete only for **1–3**. The FSRs for the MoW members of this triad are 1.04, 1.05, and 1.03, respectively. In comparison, the FSRs are 1.07, 1.08, and 1.06 for the Mo_2 and 1.04, 1.04, and 1.03 for the W_2 members of the triad. The differences in these values are small but reflect the fact that by and large the structural properties of the MoW complexes can be linearly interpolated between those of the two homonuclear homologs. Selected molecular dimensions for **1–3** and their homonuclear homologs are listed in Table IX.

Variations in Phosphine Basicities. There are two pairs of compounds which lend themselves to this comparison, $MoWCl_6(\mu\text{-dppm})_2$ and $MoWCl_6(\mu\text{-dmpm})_2$, and $MoWCl_6(dppe)_2$ and $MoWCl_6(dmpe)_2$.[27] There are slight systematic variations in the M–P, M–Cl_t, and M–Cl_b distances between these complexes. These variations are easily attributed to the M–P donor bonding ability and trans influence of the various atoms and have previously been discussed.[8]

The most important result of changing from dmpR to dppR (R = e or m) is that the M–M bond length increases, by 0.05 and 0.01 Å for the dppm and dppe compounds, respectively. These increases in the M–M bond length may be attributed to the lower basicity of the dppR ligands, which results in a greater positive charge on the metal atoms. This in turn causes some contraction in the metal d orbitals so as to decrease the overlap across the M–M gap and produce a weaker and longer M–M bond.

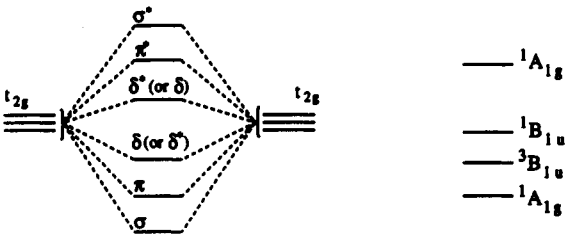

(a) Orbital Energy Level Diagram (b) State Energy Level Diagram

Figure 4. Qualitative orbital energy and state energy level diagrams for edge-sharing bioctahedral complexes.

Magnetic Behavior. The magnetic behavior of these molecules will be determined by the electronic states that are thermally accessible. Because of the very similar energies of the δ and δ* orbitals, several states must be considered.[28] Although the relative energies of the δ and δ* orbitals are uncertain, the qualitative pattern of states to be considered is predictable.[2,28] In Figure 4a the two possible patterns of MO energies to be considered are shown. A little reflection will show that the expected pattern of states, Figure 4b, is the same in both cases. The lowest and highest states will be $^1A_{1g}$, and between these states there are the $^3B_{1u}$ and $^1B_{1u}$ states, in the order shown, arising from the $\delta\delta^*$ configuration. The magnetic susceptibility that arises from a molecule that has energy levels corresponding to the diagram shown in Figure 4 may be derived from the Van Vleck formula[28] and is given in eq 1, where $x_1 = E(^3B_{1u})/kT$, $x_2 = E(^1B_{1u})/kT$,

$$\chi = \frac{Ng^2\mu_B{}^2}{kT}\,\frac{2e^{-x_1}}{1 + 3e^{-x_1} + e^{-x_2} + e^{-x_3}} \qquad (1)$$

$x_3 = E(^1A_{1g}^*)/kT$, and all of the other parameters have their usual meaning. Magnetic susceptibility data for several ESBO compounds have previously been modeled using this formula.[6,28,29] However, these measurements require large quantities of pure samples, and sophisticated susceptometers (e.g. SQUIDS), in order to produce accurate results.

Luckily, the temperature-dependent magnetic behavior of these molecules also has ramifications in certain spectroscopic features of these complexes.[4] The $^{31}P\{^1H\}$ NMR spectra of these complexes exhibit temperature-dependent chemical shifts. This dependence may in turn be used to establish the magnitude of the singlet–triplet gap using variable-temperature $^{31}P\{^1H\}$ NMR chemical shift data and eq 2,[30–32] where $\gamma_{(N)}$ is the gyromagnetic ratio of the nucleus, $H_{0(N)}$ is the resonance frequency of the nucleus, g

(24) Cotton, F. A.; Favello, L. R.; Luck, R. L.; James, C. A. *Inorg. Chem.* **1990**, *29*, 4759.
(25) Cotton, F. A.; Koch, S.; Millar, J. *J. Am. Chem. Soc.* **1977**, *99*, 7372.
(26) Pauling, L. C. *The Nature of The Chemical Bond*; Cornell University Press: Ithaca, NY, 1960.
(27) Cotton, F. A.; Eglin, J. L.; James, C. A. To be published elsewhere with other related compounds.
(28) Hopkins, M. D.; Gray, H. B.; Miskowski, V. M. *Polyhedron* **1987**, *6*, 705.
(29) Cotton, F. A.; Daniels, L. M.; Dunbar, K. R.; Falvello, L. R.; O'Connor, C. J.; Price, A. C. *Inorg. Chem.* **1991**, *30*, 2509.
(30) Campbell, G. C.; Haw, J. F. *Inorg. Chem.* **1988**, *27*, 3706.
(31) Campbell, G. C.; Reibenspies, J. H.; Haw, J. F. *Inorg. Chem.* **1991**, *30*, 171.

$$H_{obs} = H_{dia} + \frac{2g\beta H_{0(N)}A}{(\gamma_{(N)}/2\pi)kT}(3 + e^{2J/kT})^{-1} \quad (2)$$

and β are the Landé splitting factor and Bohr magneton for an electron, A is the hyperfine coupling constant between the electron and the nucleus in question, H_{dia} is the resonance frequency of the nuclei in an equivalent diamagnetic environment, $2J$ is the singlet–triplet gap in the molecule, and the remainder of the terms have their usual meaning. Several assumptions are made in describing the temperature dependence of the chemical shift in terms of eq 2. The first and most important is that excited states of higher energy do not contribute significantly to the magnetic properties. This would seem to be a valid assumption considering the relatively high energies of the other excited states compared to that of the triplet state and the results obtained from the fitting of magnetic susceptibility data. The second important assumption concerns the metal-centered dipolar contributions (ΔH^M) to the paramagnetic shifts. These dipolar contributions may be estimated utilizing eq 3,[30-32] where ω is the angle between the electron–

$$\frac{\Delta H_M}{H_0} = \frac{2\beta^2}{3kTR^3}(g_\parallel^2 - g_\perp^2)(1 - 3\cos^2\omega)(3 + e^{2J/kT})^{-1} \quad (3)$$

nucleus vector and the metal–metal bond axis of the complex and R is the electron–nucleus distance. The metal-centered dipolar shifts estimated using eq 3, the crystallographic data, and estimated values for $g_\parallel$ and $g_\perp$ are too small to contribute significantly to the observed shifts and were subsequently ignored.

Figures 5 and 6 are plots of the chemical shifts, both Mo–P and W–P, versus temperature for $MoWCl_6(dppe)_2$ and $MoWCl_6(\mu\text{-dppm})_2$, respectively. The squares indicate experimental data while the curve is the theoretical fit. The values of $-2J$, H_{dia}, and A were calculated by using a multiple parameter, nonlinear least-squares procedure to fit the variable-temperature $^{31}P\{^1H\}$ NMR data to eq 2. The fits were constrained so that both the Mo–P and W–P data gave the same $-2J$ value but individual values of A and H_{dia} were obtained. Calculated parameters for **1–3**, as well as their homonuclear analogs, are listed in Table X.

The $-2J$ values are the same order of magnitude as the values reported in the literature for some of the homonuclear complexes obtained from bulk magnetic susceptibility measurements (Table X).[6,33] It is worthwhile to point out that since NMR methods probe local magnetic effects, the values of $-2J$ determined in this way, unlike those from bulk susceptibility measurements, are not sensitive to traces of paramagnetic impurities.[34] The errors for the $-2J$ values determined from bulk susceptibility measurements were estimated to be 100 cm^{-1}, while the errors reported here are all less than 50 cm^{-1}.[6]

It is of interest that the magnitudes of the singlet–triplet gaps derived from the chemical shift data for the heteronuclear compounds fall between those for the homonuclear analogs. Also, the hyperfine coupling constants for the respective Mo–P and W–P ends of the molecules are similar in magnitude to those of the appropriate homonuclear complex. In fact, in the case of $MoWCl_6(dppe)_2$ the gap is essentially an average of the gaps of the dimolybdenum and ditungsten complexes. This would seem to be yet another example of the averaging of molecular properties in heteronuclear compounds.

Metal–Metal Bonding. The question of how the d^3–d^3 configurations interact with one another is a major topic of interest in the study of Mo_2^{6+} and W_2^{6+} complexes and has been discussed in detail in several publications.[2,6,8,28]

The MoW^{6+} complexes are subject to the same constraints and considerations as the Mo_2^{6+} and W_2^{6+} complexes. The accurate determination of the singlet–triplet gaps indicates that the δ^* to δ or δ to δ^* separation is small. Therefore, these orbitals

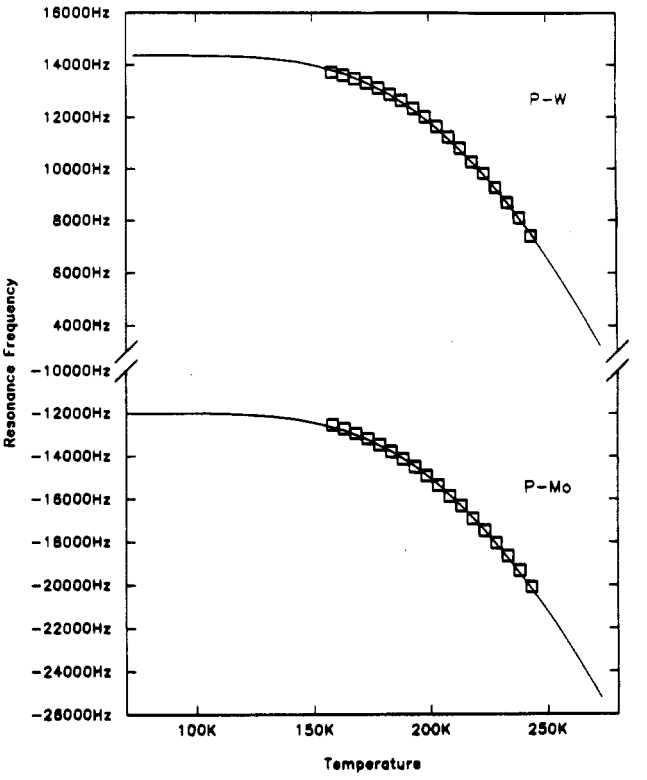

Figure 5. Plot of phosphorus chemical shifts vs absolute temperature for $MoWCl_6(dppe)_2$. The boxes are the experimental points, and the solid curves are theoretical fits.

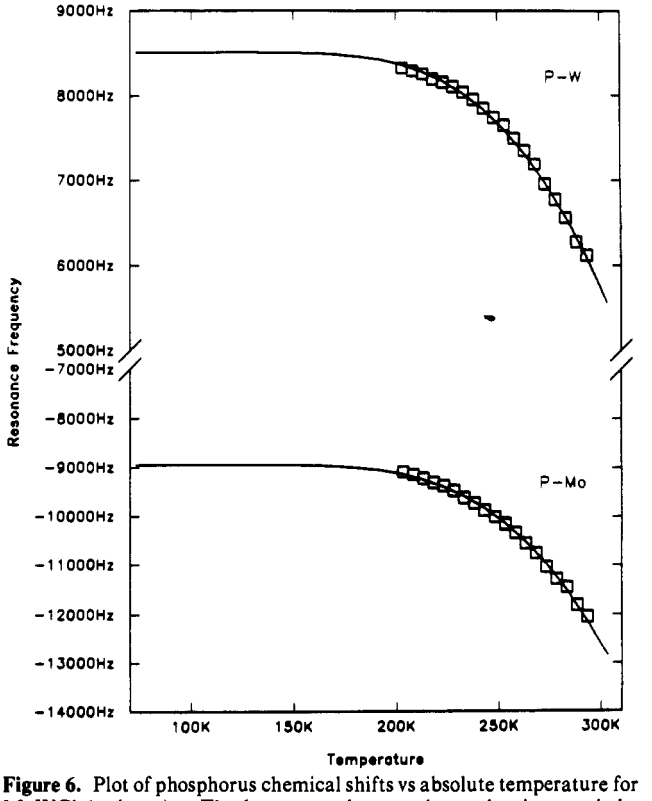

Figure 6. Plot of phosphorus chemical shifts vs absolute temperature for $MoWCl_6(\mu\text{-dppm})_2$. The boxes are the experimental points, and the solid curves are theoretical fits.

(32) (a) Boersma, A. D.; Phillipi, M. A.; Goff, H. M. *J. Magn. Reson.* **1984**, *57*, 197. (b) Holm, R. H.; Hawkins, C. J. In *NMR of Paramagnetic Molecules*; La Mar, G. N.; Horrocks, W. D., Holm, R. H., Eds.; Academic Press: New York, 1973; Chapter 7.
(33) Cotton, F. A.; Extine, M.; Gage, L. D. *Inorg. Chem.* **1978**, *17*, 172.
(34) Labauze, G.; Livage, J.; Samuel, E. *Inorg. Chem.* **1980**, *19*, 1384.
(35) Cole, N. F.; Derringer, D. R.; Fiore, E. A.; Knoechel, D. J.; Schmitt, R. D.; Smith, T. J. *Inorg. Chem.* **1985**, *24*, 1978.
(36) Canich, J. M.; Cotton, F. A. *Inorg. Chim. Acta* **1988**, *142*, 69.

Table X. Calculated Magnetic and Electronic Parameters for $M_2X_6(L\text{-}L)_2$ Complexes

complex	$-2J$,[a] cm^{-1}	A, MHz	H_{dia}, ppm
$MoW(\mu\text{-}Cl)_2Cl_4(dppe)_2$	-940 (40)	P-Mo = 40.4 P-W = 34.1	P-Mo = -148.3 P-W = 177.0
$MoW(\mu\text{-}Cl)_2Cl_4(dppm)_2$	-1430 (40)	P-Mo = 91.6 P-W = 69.4	P-Mo = -110.5 P-W = 105.0
$MoW(\mu\text{-}Cl)_2Cl_4(dmpm)_2$	-1430 (40)	P-Mo = 221.1 P-W = 103.9	P-Mo = -124.0 P-W = 96.4
$Mo_2(\mu\text{-}Cl)_2Cl_4(dppe)_2$	-1090 (40) [941]	70.6	32.2
$W_2(\mu\text{-}Cl)_2Cl_4(dppe)_2$	-840 (10) [1115]	37.6	6.1
$Mo_2(\mu\text{-}Cl)_2Cl_4(dppm)_2$	-1460 (30) [2800]	71.3	1.2
$W_2(\mu\text{-}Cl)_2Cl_4(dppm)_2$	-1230 (20)	64.2	-13.4
$Mo_2(\mu\text{-}Cl)_2Cl_4(dmpm)_2$	-1510 (20)	126.7	-10.5
$W_2(\mu\text{-}Cl)_2Cl_4(dmpm)_2$	-1130 (30)	65.6	-22.1

[a] Numbers in brackets were obtained from magnetic susceptibility data. Numbers in parentheses are estimated errors.

Table XI. Comparison of Electronic Absorption Data for $M_2X_6(L\text{-}L)_2$ Complexes

	abs bands, nm M-M unit		
compd	Mo-W	Mo-Mo	W-W
$M_2Cl_6(dppe)_2$	480	743, 507[35]	478[36]
$M_2Cl_6(dppm)_2$	495	758, 532[35]	465[36]
$M_2Cl_6(dmpm)_2$	505		

may be considered to be nonbonding in character and the bond order in these complexes is effectively two. The double-bond interpretations arises from the fact that σ and π levels are doubly occupied. This is the same conclusion previously reached for a series of $Mo_2(\mu\text{-}SR)_2Cl_4(L\text{-}L)_2$ compounds on the basis of both structural and theoretical data.[28]

Electronic Spectra. In the visible region of their electronic spectra, all the ESBO complexes display a prominent absorption band between 450 and 550 nm.[4,33] The exact origin of this absorption is unknown, but comparisons in the series indicate that the position of this band is dependent on the nature of the metal center. All of the complexes also display strong ligand-to-metal charge-transfer bands below 400 nm. Table XI contains a comparison of electronic absorptions for several heteronuclear and homonuclear ESBO compounds.

$^{31}P\{^1H\}$ NMR Analysis. The identities of these heteronuclear complexes are readily established by their distinctive $^{31}P\{^1H\}$ NMR spectra. At sufficiently low temperatures, -100 °C, all of these complexes exhibit two virtual triplets of equal integrated intensities, which identify them as heteronuclear species. These virtual triplets are due to coupling between inequivalent phosphorus atoms on the molybdenum and tungsten ends of the molecule. The magnitudes of the P-P couplings are listed in Table I. Similar coupling has been observed in quadruply bonded heterobimetallic complexes.[9,24] The $^{31}P\{^1H\}$ NMR diamagnetic chemical shift data for **1–3** and the analogous dimolybdenum and ditungsten complexes have been listed in Table XII.

Table XII. Comparison of $^{31}P\{^1H\}$NMR Chemical Shifts for $M_2X_6(L\text{-}L)_2$ Complexes

	M-M unit					
	Mo-W			Mo-Mo and W-W		
compd	δ(P-Mo)	δ(P-W)	δ(P-Mo) - δ(P-W)	δ(P-Mo)	δ(P-W)	δ(P-Mo) - δ(P-W)
$M_2Cl_6(dppe)_2$	-145.3	174.9	320.2	32.2	6.2	26.0
$M_2Cl_6(dppm)_2$	-110.6	105.0	215.6	1.2	-13.4	14.6
$M_2Cl_6(dmpm)_2$	-123.3	96.1	219.4	-10.5	-22.1	11.6

The magnitudes of the chemical shift differences between the phosphorus ligands on the different metals in the heteronuclear ESBO complexes range from 215.0 to 325.3 ppm. These chemical shift differences are extremely large compared with the differences observed in heteronuclear quadruply bonded complexes range from 24.1 to 40.2 ppm. The differences observed in quadruply bonded complexes have been attributed to a combination of paramagnetic effects and diamagnetic screening effects.[24] The introduction of a low-lying paramagnetic excited state would be likely to increase the contribution of the paramagnetic effect causing the large differences seen in ESBO complexes, but the exact cause of the differences is uncertain. The absolute differences between such chemical shifts for **1–3** and the analogous homonuclear complexes with the same bidentate phosphines are listed in Table XII.

In all cases, the downfield pattern has been tentatively assigned to the phosphorus atoms on tungsten and the upfield pattern has been assigned to the phosphorus atoms on molybdenum. The assignments were made on the basis of comparisons to positions of resonances in quadruply bonded heteronuclear complexes as no ^{183}W satellites could be observed.[9,24]

^1H NMR Analysis. Although **1–3** are only sparingly soluble in CD_2Cl_2 and slightly paramagnetic at room temperature, acceptable ^1H NMR spectra were obtained. The ^1H NMR spectra of complexes **1–3** exhibit multiplets for each of the different types of protons. These multiplets are unresolvable due to broadening from paramagnetism and the complexity of the coupling. The phenyl and methyl protons of the phosphine ligands are seen as multiplets between δ 7.0 and 8.0 and 1.3 and 1.5 ppm, respectively. The methylene and ethylene resonances appear as a multiplet between δ 2.1 and 3.3 ppm with no observable P-H coupling. The positions of the multiplets are listed in Table I.

Acknowledgment. We are grateful to Dr. Larry R. Falvello for assistance in X-ray crystallography and to the National Science Foundation for support.

Supplementary Material Available: Tables of full crystallographic data, complete bond distances and bond angles, hydrogen atom positional parameters, and anisotropic thermal parameters and labeled ORTEP projections showing the phenyl rings of the ligands (22 pages). Ordering information is given on any current masthead page.